Plasticity Considerations in Probabilistic Ceramic-to-Metal Joint Design

D. A. ONeil

J. H. Selverian

Central Research and Development,
OSRAM Sylvania Inc.,
71 Cherry Hill Drive,
Beverly, MA 01915

K. S. Kim

Division of Engineering,
Brown University,
Providence, RI 02912

A new probabilistic failure criterion was developed for the design of high-temperature ceramic-to-metal joints. The essential feature of the theory is the inclusion of the energy dissipated during plastic deformation of the adjacent braze layer in the joint. A large number of bimaterial interface fracture simulations were performed for different crack positions and orientations near the bimaterial interface to determine the effect on stresses in the ceramic near the interface. The effective stress values were then ported to a probabilistic failure analysis code, which permitted simple inclusion of the new failure criterion. Brazed joints were made and failure tested in torsion to verify the failure criterion. Results show that the new failure criterion more closely approximates the failure of the ceramic-to-metal joints over the entire range of ultimate loads, and is a significant improvement in the failures criteria previously used for this type of joint design. Aspects of the failure criterion, material systems, residual stresses, mechanical behavior, and strength predictions will be presented.

Introduction

Ceramic materials are being developed for use in advanced heat engine applications. A key issue in their design and manufacture is joining the ceramic rotor to a metal shaft to transmit power. Design concepts for ceramic-to-metal joints were described in an earlier paper (Selverian et al., 1992).

The goals of this work were to develop new methods for the design and analysis of ceramic-to-metal joints, to predict performance of the joint, and to construct and test ceramic-to-metal joints that could support a 20.9 N-m (50 MPa) torque load at 650°C and 950°C with a braze area of 2.0 cm^2. Some expectation of the strength of the ceramic joint was necessary so that different joint geometries and materials could be explored without the difficulty of making each different design. The difficulty with realizing a predictive design tool for these joints was the probabilistic nature of the ceramic material properties, and the interaction between the metal, ceramic, and braze materials.

The heat engine applications of the joints considered here are primarily loaded with high-temperature torsional stresses. Therefore, the test joints were evaluated in torsion, torsional fatigue, and thermal fatigue tests. At the completion of the work, it was desired to not only have a prototype joint design manufactured, but also to confirm the analytical models derived for joint design by comparison with life-tests of the final joint prototypes.

Experimental Procedure

Material Systems. A detailed discussion of the material systems used here is given by Selverian et al. (1994). For the 650°C application an Fe-based superalloy, Incoloy 909, was selected because of its low coefficient of thermal expansion (CTE) as well as its high-temperature properties. For the 950°C application a Ni-based superalloy, Inconel 718, was chosen solely for its high-temperature capabilities. The CTE of Inconel 718 is approximately 50 percent greater than that of Incoloy 909. In the remainder of the paper Incoloy 909 and Inconel 718 together are referred to as structural alloys.

Silicon nitride (Si_3N_4 + 6 percent Y_2O_3) was selected as the structural ceramic material. The silicon nitride shaft was polished to a 0.1 mm surface finish. A 3-mm-thick Ti-coating was electron beam evaporated onto one end of the silicon nitride shaft. This Ti coating served to promote wetting and adhesion between the ceramic and braze alloy.

Nickel and molybdenum were used as interlayer materials between the ceramic and the structural alloy, and a Au-5Pd-2Ni (in wt %) braze alloy was used. The two material systems studied were Si_3N_4/Ni/Incoloy 909 as the 650°C system and Si_3N_4/Mo/Inconel 718 as the 950°C system. The Au-5Pd-2Ni braze alloy was used in both systems.

Joint Geometry. Several ceramic-to-metal braze joint configurations were studied in the initial phases of this work. Geometries included butt, tapered and cylindrical type joints, and are detailed by Selverian et al. (1992). Stress analysis and manufacturing/brazing considerations, as well as material interaction, pointed to the cylindrical configuration for further consideration. Subsequent manufacture, experimental joint testing, and modeling considerations were focused on the following cylindrical joint geometry:

The joint consists of a 1.27-cm-dia. silicon nitride rod brazed to a 1.946 cm outer diameter metal shaft with a 2.0 cm^2 brazed area. The ceramic rod fits into a cup machined into the end of the metal shaft. A schematic of the ceramic-to-metal joint geometry is shown in Fig. 1.

Testing of Brazed Joints. Figures 2(*a*) and 2(*b*) show a brazed joint between silicon nitride and Incoloy 909. This type of joint was used for the torsion and torsion fatigue tests. All of the mechanical testing of the brazed joints was carried out on a servohydraulic axial/torsional machine. The top and bottom gripping axes were axially aligned to within 40 μm of one another. Torsion load to failure and fatigue torsion tests were performed on the brazed joints; all tests were performed in air. Details of the torsion test procedures are given by Selverian et al. (1994). The results for the tests are given in Tables 1–4.

In Tables 1–4 one of the failure modes is described as "slippage." Slippage here refers to excessive relative rotational motion between the ceramic and superalloy parts of the joint such that the test had to be stopped. One of these failure surfaces

Contributed by the International Gas Turbine Institute and presented at the 39th International Gas Turbine and Aeroengine Congress and Exposition, The Hague, The Netherlands, June 13–16, 1994. Manuscript received by the International Gas Turbine Institute February 26, 1994. Paper No. 94-GT-229. Associate Technical Editor: E. M. Greitzer.

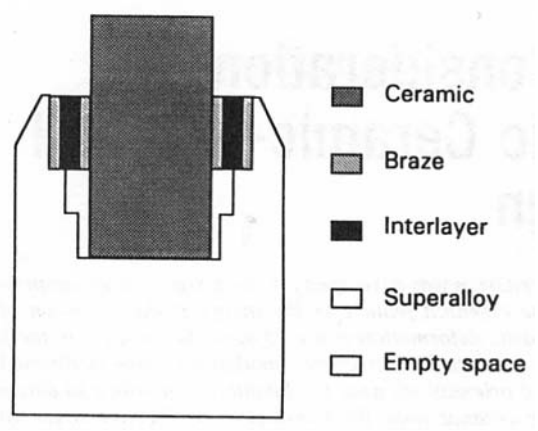

Fig. 1 Schematic of the ceramic-to-metal joint geometry

was examined by Auger spectroscopy. This revealed that the failure occurred in the near-interfacial regions; braze, ceramic, and reaction zone products were observed. As detailed by Selverian et al. (1994), at elevated temperatures (when the shrink-fit stresses become tensile) the brittle interfacial reaction zone fails. This result was predicted by Selverian et al. (1993).

Torsion tests were run at a rate of 0.2°/s and the axial load was controlled to within ±4.5 N of zero to maintain pure torsional loading. An induction furnace, with a SiC susceptor, was used to heat the joints for the elevated temperature tests. Torsion fatigue tests were carried out at minimum and maximum torques of 3.95–20.9 N-m, 6.0–31.7 N-m, or 8.0–42.2 N-m, all with a 1.5 Hz loading frequency. Torques of 3.95–20.9 N-m are typical values found in heat engines currently under development.

The temperature versus time profile used for the 650°C thermal fatigue testing consisted of a maximum temperature of 650°C and a minimum temperature of 335°C with a frequency of 0.07 Hz. The temperature versus time profile used for 950°C thermal fatigue testing consisted of a maximum temperature of 950°C and a minimum temperature of 545°C with a frequency of 0.11 Hz. The thermal fatigue conditions were also developed with the idea of simulating the stresses developed in a heat engine. All the mechanical and thermal tests were conducted in air.

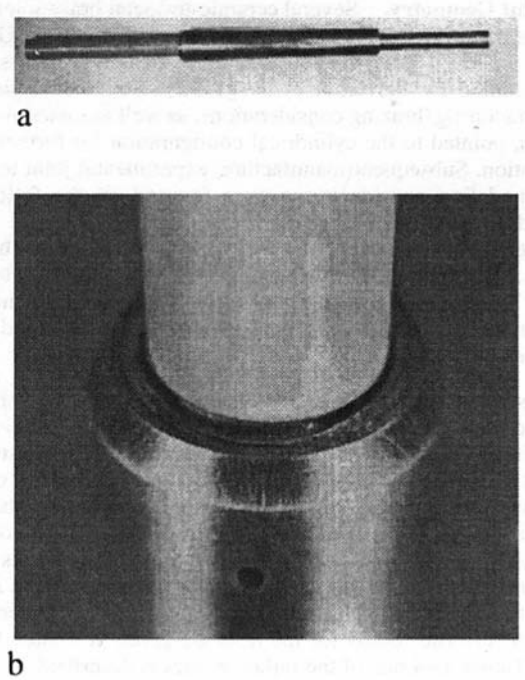

Fig. 2 Brazed Si_3N_4/Ni/Incoloy 909 joint. Test sample for torsion and mechanical fatigue testing. The ceramic is 1.27 cm in diameter and the metal is 1.946 cm in diameter.

Table 1 Results of the torsion tests of Si_3N_4/Ni/Incoloy 909 brazed joints

Test Temp. (°C)	Torque (N-m)	Shear Strength (MPa)	Bending Moment (N-m)	Rotation (°)
25	61	151*	7	2.22
	97	242*	14	3.52
	53	132*	11	1.98
	30	75*	13	1.15
	60	148*	10	1.05
	49	121*	23	2.55
	64	158*	14	3.05
	90	222*	12	4.3
	45	111*	2	2.05
650	4.	11.5#	---	---
	1.6	3.9#	---	0.10
	7.0	17.4#	---	---
	4.9	12.1#	---	0.21°

* broke in ceramic.
# ceramic slipped in joint.

Fatigue Testing. Thermal and mechanical fatigue tests were used to evaluate the effects of repeated thermal and mechanical loading on the long-term performance of the brazed joints. Brazed joints were made for thermal fatigue tests at 650°C and 950°C. The same joint geometry was used as in Fig. 1. The initial crack distribution in the joint was checked by microfocus x-ray. No cracks were detected in the silicon nitride. The apparent lack of cracks in the silicon nitride could be due to either no cracking or to the cracks being smaller than the 40 mm detection limit of the x-ray equipment. The samples were

Table 2 Results of the torsion tests of Si_3N_4/Mo/Inconel 718 brazed joints

Test Temp. (°C)	Torque (N-m)	Shear Strength (MPa)	Bending Moment (N-m)	Rotation (°)
25	12	30	25*	0.38
	40	98	13*	1.19
	23	56	17*	0.70
	51	127	16*	0.80
	41	101	16*	0.64
950	0.34	0.84#	---	---

* broke in ceramic.
# ceramic slipped in joint.

Table 3 Room temperature fatigue tests of Si_3N_4/Ni/Incoloy 909 and Si_3N_4/Mo/Inconel 718 brazed joints

Joint	Torque (N-m)	Rotation (°)	Number of Cycles for Failure
Si_3N_4/Ni/ Incoloy 909	3.95-20.9	±0.31	> 10^3*
	"	±0.32	> 10^3*
	"	±0.31	> 10^3*
	"	±0.32	> 10^3*
	"	±0.31	> 10^6
	6.0 - 31.7	---	> 10^6
	8.0 - 42.2	---	> 10^6
Si_3N_4/Mo/ Inconel 718	3.95 - 20.9	---	> 10^3*
	"	±0.26	> 10^3

* These samples were heated to 650-700°C, then gripped in the testing machine, and then cooled to room temperature before testing, to realign the sample. These samples were stopped at 10^3 cycles due to time limitations, not failure of the joint.

reexamined by microfocus x-ray after 10, 100, and 1000 cycles. The Si_3N_4/Ni/Incoloy 909 joints survived all 1000 cycles without evidence of cracking. Severe oxidation of the molybdenum interlayer in the Si_3N_4/Mo/Inconel 718 joints prevented their complete testing.

Several Si_3N_4/Ni/Incoloy 909 and Si_3N_4/Mo/Inconel 718 joints were torsion fatigue tested at room temperature, Table 3. A Si_3N_4/Ni/Incoloy 909 joint was first fatigued at room temperature for 10^3 cycles then fatigued at room temperature for 10^6 cycles. All the joints survived 10^6 fatigue cycles at a torque amplitude of 3.95–20.9 N-m. The joints showed no signs of degradation; the rotation required to maintain these torques was unchanged at ±0.32 deg from the start of the test. The torque amplitudes were increased to 6.0–31.7 N-m and to 8.0–42.2 N-m. One joint was tested at each torque level and joints survived 10^6 cycles, Table 3.

The joints that failed in the ceramic were compared to modeling predictions of the joint strength. Since the new failure criterion is applicable only in brittle materials having a distribution of strengths, the experimental failures due slippage were not included in the experimental failure distribution.

Modeling Approach

Previous work (Selverian et al., 1994) has shown the applicability of probabilistic failure analysis in the design of ceramic components. As a result of this work, the mode of failure in the ceramic material was qualitatively known by failure surface and location of initiation (using various microscopy methods). However, the probabilistic failure methods used by Nemeth et al. (1989) (which were used in previous ceramic-to-metal joint designs) do not include energy dissipation by plastic work. Plastic energy was dissipated in the braze layer during cool down from the brazing temperature, and also in service conditions of the joint. Our aim here, therefore, was to consider the effect of the plasticity of the braze layer on crack propagation when the cracks are at or near the ceramic–braze interface. Once the effect on cracks near the interface was quantitatively understood, it was incorporated into the probabilistic failure analysis code as stress modification factors. By including the plasticity effect in this way, modifications to the probabilistic failure code were precluded. A discussion of the new failure criterion follows, but detailed structure of the technique is given by Kim et al. (1992), Yang and Kim (1993), and Kang et al. (1992).

It is useful to describe the reasoning behind our approach. In previous probabilistic failure analyses of the entire joint system (Selverian et al., 1992), stress results from finite element studies of the joint were post-processed through a probabilistic ceramic failure analysis code, NASA CARES (Nemeth et al., 1989). The stresses and volumes of each of the ceramic finite elements were combined with Weibull strength data for the ceramic finite elements to give the probability of failure at each position in the ceramic body. In addition, a cumulative probability of failure for the entire joint was also calculated. The drawback with this method was that of all the ceramic failure models included in the CARES code, none included the effect of having a ductile layer near the surface of the ceramic body. This ductile layer (the braze) has been shown to absorb some of the energy in the system that may be otherwise used for further crack growth.

In our current modeling work, we calculated this effective toughening of the system by evaluating the energy release rate at the crack tip (which is near the elasto-plastic interface of the ceramic–braze zone) relative to the energy release rate at a crack tip away from the interface. This series of finite element calculations can then be performed for a range of crack-tip orientations relative to the interface, and also for a range of distances of the crack-tip to the interface. Finally, these data are interfaced with the CARES probabilistic failure analysis code in the form of a new failure model specific to ceramic components joined to plastically deforming materials. The derivation of the "T-stress" component for the braze joint and some results showing the mode-dependent toughening of the interface follow.

T-Stress Component Evaluation. Work has been being carried out to evaluate the so-called T-stress at the tip of a crack at or near a bimaterial interface with one of the interface layers modeled as an elastic-strain hardening material. For a tensile specimen with a crack parallel to the tensile direction, the stress at the crack tip can be written as

$$\sigma_{\alpha\beta}(r, \theta) = \frac{K_I}{\sqrt{2\pi r}} f_{\alpha\beta}(\theta) + \sigma^o_{\alpha\beta}(\theta) + a_1 \sqrt{r} g_{\alpha\beta}(\theta) + \ldots a_2 r h_{\alpha\beta}(\theta) + a_n (\sqrt{r})^n h_{\alpha\beta}(\theta) \quad (1)$$

The first term, $(K_I/\sqrt{2\pi r}) f_{\alpha\beta}(\theta)$, is usually described as the singular term in linear elastic fraction mechanics, and the first nonsingular term is known as the T-stress, or σ_{ox} among experimentalists. So

$$\sigma^o_{\alpha\beta}(\theta) \equiv \sigma_{ox} \equiv T\text{-stress}. \quad (2)$$

Cotteral and Rice (1980) have shown the instability of the

Table 4 Results of the 500°C torsion tests of Si_3N_4/Ni/Incoloy 909 brazed joints. All of these joints were fatigued tested at room temperature before testing at 500°C.

Torque (N-m)	Shear Strength (MPa)	Previous Fatigue Test Conditions (cycles at stress)	Fracture Mode
49.7	123	10^3 at 3.95-20.9	slipped
24.8	61	10^6 at 3.95-20.9	cer. broke
15.3	38	10^6 at 6.0 - 31.7	slipped

crack path depends on the T-stress term. In addition, it has been speculated that the nonsingular term may play a significant role in crack branching. For the design of the ceramic-to-metal brazed joint, the description of the instability of the crack path due to the T-stress term will permit numerical study of the fracture surface by following crack propagation and allow joint design that takes into account the effect of this nonsingular term coupled to the elasto-plastic interface (the ceramic-braze interface). The T-stress term in further discussion refers to the first nonsingular term in the crack tip stress series description.

The method used to find the nonsingular stress term (the T-stress) at the crack tip uses an application of an energetic force on a point load in the development of an interaction (or mutual) integral to extract this term. This work is detailed in Kim (1992).

Following is the description of the general method for the study of an interaction integral of a point load. The conservation force on an object such as an inclusion, a crack tip, a dislocation, or a point force is referred to as an *energetic force* or an *energy release rate.* The energetic force, G, is defined as the negative gradient of the potential energy of a body with respect to a virtual displacement of the object. Denoting the virtual displacement of the object by $\rho\mathbf{e}$ for which $\mathbf{e}$ is a unit vector, the definition of the energetic force is expressed as

$$G = \lim_{\rho \to 0} \frac{II(\mathbf{r} + \rho\mathbf{e}) - II(r)}{\rho} \mathbf{e}, \tag{3}$$

where II represents the potential energy of the body. The energetic force often can be calculated by the $\mathbf{J}$ integral. Provided the mechanical response function, i.e., the elastic properties, are invariant in the direction of G, the energetic force, G, can be evaluated by a surface integral (or a contour integral for two dimensional cases) in terms of the field quantities. The elastic equilibrium field surrounding the object is represented by the field quantities of the stress, σ, the strain, ϵ, and the displacement, u. Denoting the equilibrium field, $\{\sigma, \epsilon; u\}$, by S, the surface integral is depicted by $\mathbf{J}_\Gamma(\mathbf{S})$, where Γ indicates the integrating surface (or contour). A Cartesian component of the $\mathbf{J}$ integral is expressed as

$$J_i = \int (Wn_i - \sigma_{kj} n_k u_{j,i}) d\Gamma, \tag{4}$$

where the summation convention is assumed on the repeated indices, the strain energy density function is represented by W and the out normal of the surface, Γ, is indicated by $\mathbf{n}$.

The energetic forces of various singular objects have many interesting properties. Those of dislocations, point defects, and cracks have been applied to many engineering problems in plasticity, diffusion, and fracture mechanics. However, not much attention has been paid to those of point forces.

The stress state around a point load in a linear elastic medium can be separated into two parts. One is the singular stress field corresponding to the point load in an infinite medium, denoted by superscript p, e.g., S^p. The remaining stress field corresponds to the image effect of the limited geometry and other sources of stresses. This remaining field is denoted without superscripts, e.g., S. In order to get a useful expression of the energetic force of a point load in such a superposed field, an alternative expression of the $\mathbf{J}$ integral of a general superposed field is derived first, and then some properties of the $\mathbf{J}$ integral related to the energetic force of a point load will be discussed next.

Consider the superposition of two general equilibrium fields, S^A and S^B. Substituting the field quantities of the total field, $S^A + S^B$, into Eq. (2), the $\mathbf{J}$ integral of the total field over a Γ is expressed as

$$\mathbf{J}_r(S^A + S^B) = \mathbf{J}_r(S^A) + \mathbf{J}_r(S^B) + \mathbf{J}^{\text{int}}_\Gamma(S^A, S^B), \tag{5}$$

where the superscript int indicates the interaction integral. A Cartesian component of the interaction integral is given by

$$\mathbf{J}^{\text{int}}_\Gamma(S^A, S^B) = \int_\Gamma (W^{\text{int}} n_i - \sigma^A_{kj} n_k u^B_{j,i} - \sigma^B_{kj} n_k u^A_{j,i}) d\Gamma, \tag{6}$$

where the interaction strain energy, W^{int}, has the relationship

$$W^{\text{int}} = \tfrac{1}{2}(\sigma^A_{ij}\epsilon^B_{ij} + \sigma^B_{ij}\epsilon^A_{ij}) = \sigma^A_{ij}\epsilon^B_{ij} = \sigma^B_{ij}\epsilon^A_{ij}. \tag{7}$$

The last two equalities hold due to the symmetry of the elastic moduli tensor. Therefore, the interaction integral can be expressed in a convenient form:

$$J^{\text{int}}_i(S^A, S^B) = \int_\Gamma (\sigma^B_{kj}\epsilon^A_{kj} n_i - \sigma^B_{kj} n_k u^A_{j,i}) d\Gamma - \int_\Gamma (\sigma^A_{kj} n_k u^B_{j,i}) d\Gamma, \tag{8}$$

Interaction Integrals for Extracting Stress Intensity Factor and *T*-Stress. In the previous section we outlined a method for evaluating the so-called T-stress component of the stress field at or near an interface crack. In this section, the method for numerically evaluating the stress field of a crack near the interface of a multilayered structure (the ceramic-to-metal braze joint) is described, especially when plastic deformation of one of the layers (the braze layer) occurs.

In order to extract the complex stress intensity factor, K, and T-stress, the interaction integral based on the path-independent J-integral is used by several authors (Moran and Shih, 1987; Kim et al., 1992). To define the interaction integral, consider two general equilibrium fields as before, S^A and S^B. The J-integral of the superposed field, $S^A + S^B$, over a contour Γ can be expressed as

$$J(S^A + S^B) = J(S^A) + J(S^B) + J^{\text{int}}(S^A, S^B) \tag{5}$$

where the superscript int indicates the interaction integral.

First, to extract the complex stress intensity factor K near an interface crack, consider an interaction integral between the actual field S (given by Eq. (1)) and the auxiliary field $S^{\tilde{K}}$, which is the $(1/\sqrt{r})$ singular field and whose strength is $\tilde{K} = |\tilde{K}| e^{i\phi}$. Then by calculating each J-integral in Eq. (5), the interaction integral $J^{\text{int}}(S, S^{\tilde{K}})$ can be expressed in terms of two stress intensity factors, K and $\tilde{K}$, as

$$J^{\text{int}}(S, S^{\tilde{K}}) = \frac{|\tilde{K}| h_{22}}{2 \cosh^2 \pi\epsilon} (K_1 \cos\phi + K_2 \sin\phi) \tag{9}$$

for an anisotropic bimaterial interface crack where h_{22} is defined by Eq. (A.10) in Choi et al. (1991). Therefore, the complex stress intensity factor can be completely obtained (i.e., K_1 and K_2 separately) by applying Eq. (9) twice with the different mode, ϕ, of the auxiliary field $S^{\tilde{K}}$, and then by solving for K_1 and K_2. In each case, the interaction integral, $J^{\text{int}}(S, S^{\tilde{K}})$, is calculated by Eq. (9).

Now, to extract the T-stress at an interface crack, consider an interaction integral between the actual field S and the auxiliary field $S^{\tilde{T}}$, which is the $(1/r)$ singular field of the point force, $\tilde{T}$, located at a crack tip and directed to x-axis. Noting that, for the in-plane problem, only the nonsingular stress at the crack tip is σ^o_{xx}, Kim et al., (1992) have shown that the interaction integral between S and $S^{\tilde{T}}$ field is reduced to

$$J^{\text{int}}(S, S^{\tilde{T}}) = \tilde{T}\epsilon^o_{xx}. \tag{10}$$

Once ϵ^o_{xx} is obtained through this equation, the nonsingular stress term σ^o_{xx} can be easily calculated using Hookes' law. Note that, for the interface cracks, the T-stress can have a jump across the interface. The jump quantities are determined from the compatibility condition that the corresponding strain ϵ^o_{xx} should be continuous across the interface.

Both fundamental fields of $S^{\tilde{K}}$ and $S^{\tilde{T}}$ in the above were presented in Choi et al. (1991) for an interface crack between

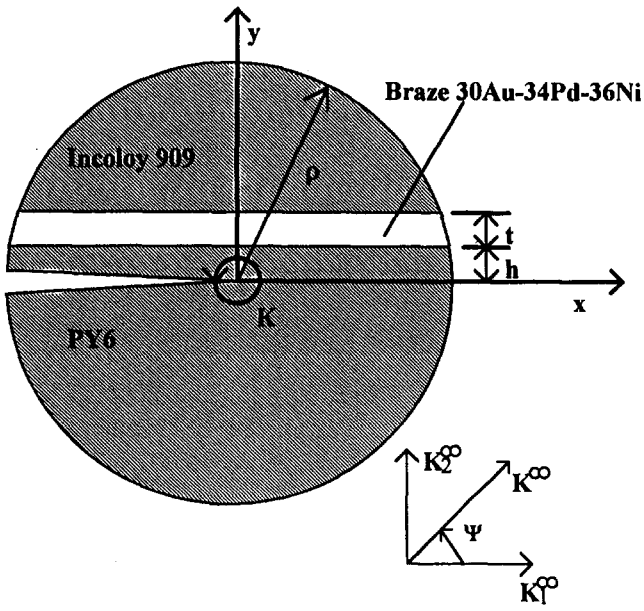

Fig. 3 Geometry of the model used to find the effect of a plastic region on bimaterial fracture in the ceramic-to-metal brazed joint. Note material system studied, and definition of h and t. In the figures, $\bar{\sigma}^{o}_{xx} = \sqrt{\rho}\sigma^{o}_{xx}/|K^{\infty}|$, and $|\bar{K}^{\infty}| = |K^{\infty}|/(\sigma_o\sqrt{\rho})$.

an anisotropic bimaterial, but they can also be used for the isotropic cases.

Toughening of the Brazing Structure. These methods have been implemented into a two-dimensional finite element program, and results obtained for the material system specific to the ceramic-to-metal joint. The geometry of the metal-braze-ceramic region is shown in Fig. 3. Material properties of each of the materials were:

1 Structural Alloy; Incoloy 909
E_s = 158.6 GPa, υ_s = 0.34
2 Braze Material; 30Au-34Pd-36Ni
E_b = 32.4 GPa, υ_b = 0.3
Yield stress σ_o = 626.0 MPa
3 Ceramic; PY6 (Si_3N_4)
E_c = 296.5 GPa, υ_c = 0.2

The distance h/t and mode mixity, Ψ, were varied over a wide range of values typical for the ceramic-to-metal braze joint. These analyses were performed using two-dimensional finite element methods. Typical results for a crack parallel to the ceramic-braze interface are shown in Fig. 4. Figure 4(a) shows the increasing energy release rate when the crack gets closer to the interface. Note also the energy release rate increases as fracture tends to mode *II* loading. The change in the *T*-stress factor for the same cases of mode mixity and crack position are illustrated in Fig. 4(b).

In summary, we have seen that not only is the interface tougher in mode *II* loading (as it is near an elastic-elastic interface), but also that the plastic deformation of braze material also acts as a toughening agent, particularly in mode *II* loading. The result is a failure model for ceramics, which is significantly different from existing models.

Detailed Description of Implementation. One goal in this work was to implement a failure condition that includes the plasticity of the braze layer into an existing probabilistic failure code, the NASA CARES program. The method by which the failure criterion is implemented into the existing FE protocol is described here.

The underlying method we used is as follows: The effective increase in energy release rate due to plasticity was calculated (via FEA techniques) for which a wide range of far-field mode mixities and distances of the crack from the braze-ceramic interface. Collecting these data onto a G versus crack distance plot (Fig. 5), a family of mode mixity points results. A best-fit curve is then passed through the points and the coefficients of these curves are used to weight the stress values calculated for the experimental joint system. These weights (described in detail below) effectively *reduce* the stress near the interface region of the ceramic, thereby decreasing the probability of failure.

The correction factor for stress was estimated using energy release data obtained from finite element calculations. Data were obtained for cracks at different distances h from the interface (with a constant brazing thickness t) under various far-field loading conditions. The ratio of the total energy release rate due to far-field loading G^{∞} to the actual energy release rate calculated at the crack tip G is a measure of the amount of energy consumed by plastic yielding in the brazing layer. The behavior of this ratio was plotted as a function of h/t for various angles of far-field loading incidence Ψ. These plots were made for different loading magnitudes $|K|$, where the magnitude has been normalized as follows (Figs. 3, 4, and 5). A detail of the stress components affected by the stress factors is shown in Fig. 6. The far-field stress intensity factor was defined as:

$$|K^{\infty}| \equiv \frac{K_{IC}}{\sigma_o\sqrt{t}} \tag{11}$$

These data show the dependence of G^{∞}/G on $|K^{\infty}|$ and h/t for each angle of incidence. Thus, the effective stresses we seek should assume this form:

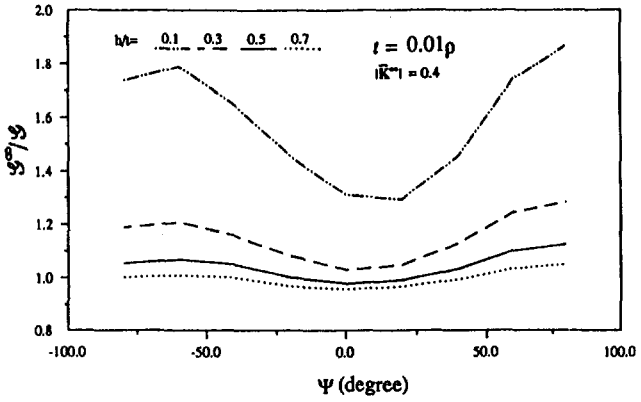

(a) Mode-dependent Toughening

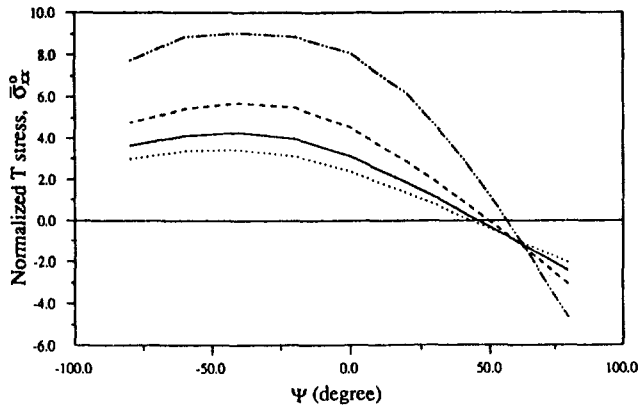

(b) T stress

Fig. 4 Toughening effect of plastic interlayer (a), and *T*-stress component values as a function of mode mixity and distance of crack tip from interface (b)

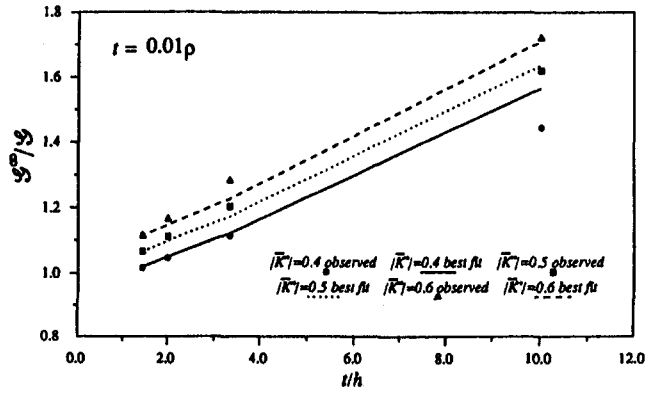

(a) Best Fit Function for Toughening Factor

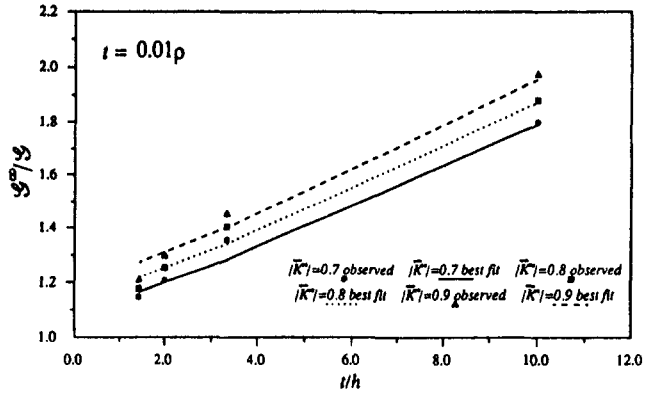

(b) Best Fit Function for Toughening Factor

Fig. 5 Best-fit curves used for stress weighting factors. These curves are specific to a given material system.

$$\sigma_{yy}^{\text{eff}} = \frac{\sigma_{yy}}{\sqrt{f_c}} \tag{12}$$

$$\sigma_{xy}^{\text{eff}} = \frac{\sqrt{\lambda}\sigma_{xy}}{\sqrt{f_c}} \tag{13}$$

$$\sigma_{zy}^{\text{eff}} = \frac{\sqrt{\lambda}\sigma_{zy}}{\sqrt{f_c}} \tag{14}$$

$$\sigma_{xx}^{\text{eff}} = \sigma_{xx}$$

$$\sigma_{zz}^{\text{eff}} = \sigma_{xz}$$

$$\sigma_{zz}^{\text{eff}} = \sigma_{zz}$$

where

$$f_c = \frac{G^{\infty}}{G} = f\left(\frac{t}{h}, |K^{\infty}|\right)$$

and

$$\lambda = 0.3$$

Notice that in the xx, xz, and zz directions, no toughening effects are considered, since the metal plasticity model affects shear coupons only (Fig. 6).

To find f_c, numerous function forms were assumed and tested using a least-squares approximation. The following exponential form was eventually settled on because it provided the best fit to the data with the smallest number of independent parameters (three):

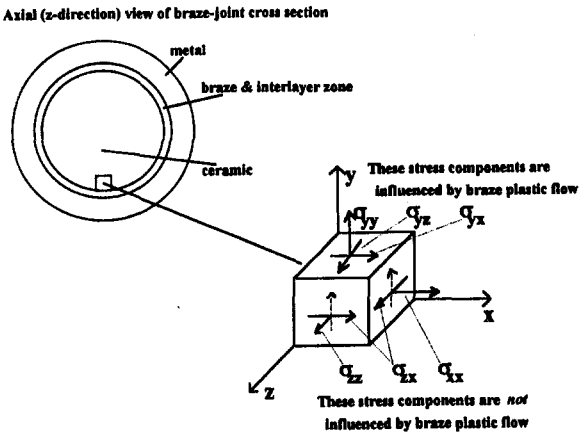

Fig. 6 Detail of stress components in the ceramic-to-metal joint affected braze layer plasticity

$$f_c = \exp\left(A\left(\frac{t}{h}\right) + B(|K^{\infty}|) + C\right) \tag{15}$$

Using data for $\psi = 0$ deg, $0.4 \leq |K^{\infty}| \leq 1.0$, and $1.44 \leq t/h \leq 10$, the least-squares approximation yields:

$$A = 0.0837$$

$$B = 0.0447$$

$$C = 0.0711$$

With these values, Eq. (15) predicts the toughness correction factor with a standard error of approximately 0.032723.

Equations (12) – (14) can now be used to modify the stress readings given the magnitude of far-field loading and the ratio of the brazing layer thickness to the distance from the interface to a crack imperfection.

Results and Discussion

An applied torque was superimposed with the calculated residual stress field as a shear stress. Figure 7 shows the torque distribution used to determine the shear stress. A stress concentration due to the change in cross section at the joint was included as before. The stress concentration was 1.7 at the top of the joint and tapered off to 1.0 a distance of one ceramic diameter away from the joint. Selection of the stress concentration factor depended on the radius of the fillet formed by the braze alloy. A fillet radius of 1 mm was selected; however, the fillet radius varied over the joint area. The stress concentration factor was estimated from Rourk (1971).

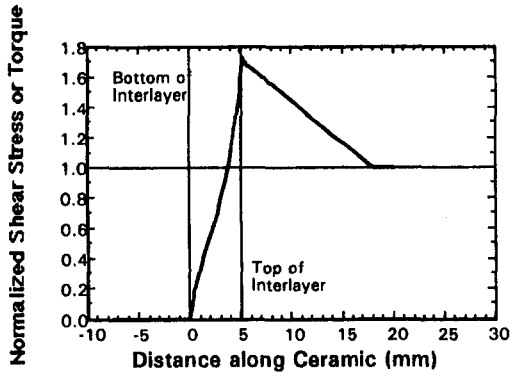

Fig. 7 Plot of the torque distribution in the ceramic portion of the brazed joint. Torque values are normalized to the applied torque.

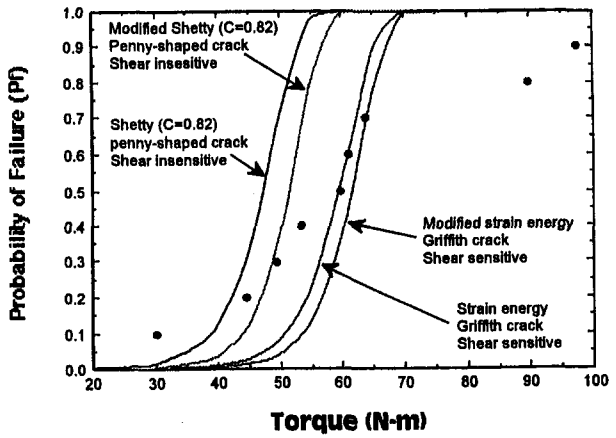

Fig. 8 Predicted and experimental values of the brazed joint strength measured in torsion (Si_3N_4/Ni/Incoloy 909). Two failure theories were used: (1) Shetty criterion with $\bar{c}$ = 0.82, penny-shaped crack, and a shear-insensitive Batdorf crack density, and (2) coplanar strain energy release rate, Griffith crack, and a shear-sensitive Batdorf crack density.

The fraction of torque carried by the ceramic and metal components in the joint region was calculated based on the material properties and was also factored into the torque distribution shown in Fig. 7. Once the torque was added to the residual stress field, the combined stress field was used as input to the CARES probabilistic failure computer code (Nemeth et al., 1989) to obtain the probability of survival for the joint at the applied torque level. This same procedure was performed at several different torques. The probability of failure (P_f) values were calculated as a function of applied torque. This probabilistic approach to joint strength, unlike a maximum principal stress approach, provided a method to estimate the strength distribution of a ceramic-to-metal brazed joint and can be used as a design aid.

Two failure theories were used to predict the behavior of the ceramic-to-metal joints for comparison. These were: (1) Shetty criterion, with $\bar{c}$ = 0.82, a penny-shaped crack, and a shear-insensitive Batdorf crack density coefficient, and (2) coplanar strain energy release rate, with a Griffith crack, and a shear-sensitive Batdorf crack density coefficient. For these failure theories the Weibull modulus (m_v), the normalized Weibull scale parameter (σ_{ov}), and the Batdorf crack density coefficient (k_{BV}) were calculated from four-point bend tests of the silicon nitride material used in the ceramic-to-metal brazed joints. Twenty-four samples were tested and 1 outlier was detected in the data (Selverian et al., 1992).

A Weibull modulus (m_v) of 21.2 and a normalized Weibull scale parameter (σ_{ov}) of 369.8 MPa(m)$^{3/21.2}$ were used for both failure theories. A shear-insensitive Batdorf crack density coefficient of 43.4 and a shear-sensitive Batdorf crack density coefficient of 22.2 were used for the Shetty and coplanar strain energy release rate theories, respectively. The maximum likelihood method was used to fit the experimental data. The constants described above were required as input variables by the CARES program and are further described by Nemeth et al. (1989).

The new failure criterion was tested on ceramic-to-metal joints containing nickel and moly interlayers with Incoloy 909 and Inconel 718 structural components, respectively. Figures 8 and 9 show the probability of failure versus applied torque on the two joint systems with experimental results. Both penny-shaped crack and Griffith crack were assumed to find the failure envelope. The new model shifted the failure curves, resulting in a less conservative failure prediction for both joint systems, and for both penny-shaped and Griffith cracks. The reason for the shift in new model (or "modified" as indicated on Figs. 8 and 9) was that previous models did not account for the fracture energy absorbed by plastic work of an adjoining material (the braze layer). Therefore, it predicted that a larger applied torque could be tolerated for a specified probability of failure. It is to be noted that, especially for the Incoloy 909 material system, the new failure model predicts the experimental results more closely. It is believed that the new failure model will provide more accurate prediction for ceramic failure where some plastic work is encountered in manufacturing or service.

In Figs. 8 and 9, the predicted strength distributions surrounded the experimental values and intermediate values of P_f, where $P_f = 1 - P_s$. However, at the low and high regions of the probability distributions, the predictions deviated from the experimentally measured strengths. Also, the predicted probability distributions were much steeper (higher Weibull modulus) than the experimental probability distribution. The Weibull modulus decreased from 21.2 for the unbrazed ceramic to ~4 for the Si_3N_4/Ni/Incoloy 909 brazed joints. A similar decrease in Weibull modulus was seen in shear testing of ceramic-to-metal lap joints (Selverian et al., 1992) and in four-point bend tests of ceramic-to-metal butt joints. The cause of the difference in the slopes (Weibull modulus) of the probability distributions was unknown.

Summary

Material systems designed for 650°C and 950°C applications were evaluated in terms of torsion, torsion fatigue, and thermal fatigue. Si_3N_4/Ni/Incoloy 909 was selected as the 650°C system while Si_3N_4/Mo/Inconel 718 was selected as the 950°C system. The Au-5Pd-2Ni braze alloy was used in both systems. A cylindrical cup joint geometry with an interlayer was selected for these joints.

Room temperature and 500°C torsion strengths of the 650°C system were measured in the range of 30–100 N-m with a 2 cm^2 brazed area while the strength at 650°C was significantly lower (1.6–7.0 N-m). This was attributed to a reduction in the shrink-fit at 650°C (Selverian et al., 1992). The Si_3N_4/Ni/Incoloy 909 joints showed excellent room temperature fatigue behavior. A similar trend was seen in the high-temperature strength of the Si_3N_4/Mo/Inconel 718 joints, which had lower strength than the Si_3N_4/Ni/Incoloy 909 joints due to the high CTE of Inconel 718.

A new failure criterion, based on the energy dissipated by plastic deformation of the braze material, was developed. A wide range of finite element calculations varying the position of the crack from the interface, and varying the mode mixity

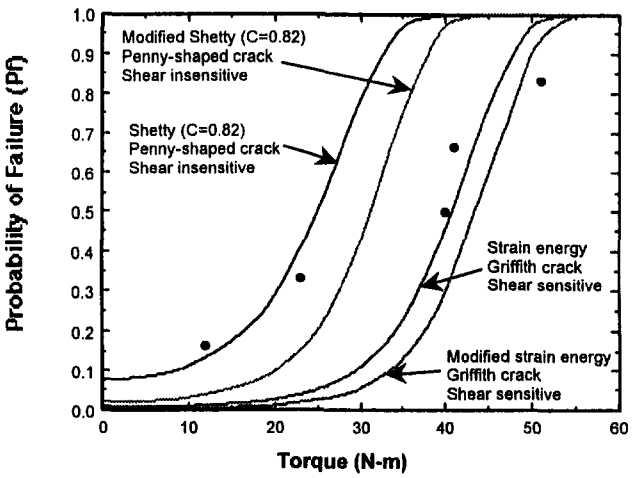

Fig. 9 Predicted and experimental values of the brazed joint strength measured in torsion (Si_3N_4/Mo/Inconel 718). Two failure theories were used: (1) Shetty criterion with $\bar{c}$ = 0.82, penny-shaped crack, and a shear-insensitive Batdorf crack density, and (2) coplanar strain energy release rate, Griffith crack, and a shear-sensitive Batdorf crack density.

of the crack, were performed. These analyses provided the effective toughening factors near the interface due to the plastic deformation of the braze material. Using these toughening values, the new failure criterion was simply integrated into an existing probabilistic failure analysis code by including the energy absorption as stress factors on stress components, which were affected by permanent braze deformation. The criterion showed better fit to the experimental joint failure statistics than the existing failure criteria in the probabilistic code. Probabilistic failure predictions for ceramic materials adjacent to plastically deforming materials should include this factor.

The strength predictions of the finite element analysis were compared with experimental results. Scatter in the measured strengths and the difference between measured and predicted strengths indicated the importance of processing effects and the probabilistic nature of ceramic failure on the fracture process. However, the probabilistic approach for the ceramic-to-metal brazed joints was a better method for comparing the performance of various brazed joints due to the statistical nature of ceramic failure, and it provided an estimate of the strength distribution of the joint for design considerations. The new failure criterion provided better guidelines for constructing high-temperature ceramic-to-metal joints than previous models. The model is best applied to ceramic components where the failure of the ceramic is affected by plastic deformation of nearby materials.

Acknowledgments

This research was sponsored, in part, by the U.S. Department of Energy, Assistant Secretary for Conservation and Renewable Energy, Office of Transportation Systems, as part of the Ceramic Technology for Advanced Heat Engines Project of the Advanced Materials Development Program, under contract DE-AC05-840R21400 with Martin Marietta Energy Systems, Inc. Special thanks go to M. Santella and D. R. Johnson at ORNL. The support of R. Schulz at the DOE is also appreciated.

The authors wish to thank H. Kim for his support and contributions. The participation in the experimental program by D. Bazinet and G. McCloud is gratefully acknowledged. A significant contribution to program management and braze alloys was made by Shinhoo Kang, Dept. of Inorganic Materials Engineering, School of Engineering, Seoul National University, Seoul, Korea.

References

Choi, H. C., Kim, K. S., and Shih, C. F., 1991, "A Study on Interlayer Effect on Interface Toughness, Parts I & II," ASME *Journal of Applied Mechanics,* Vol. 58.

Cotterall, B., and Rice, J. R., 1980, "Slightly Curved or Kinked Cracks," *Int. Journal of Fracture Mechanics,* Vol. 16, pp. 155–169.

Kang, S., Selverian, J. H., and O'Neil, D., 1992, Oak Ridge National Laboratory, Final report, Subcontract No. 86X-SB047C.

Kim, K. S., Stigh, U., and Choi, H. C., 1992, "A Study of the Energetic Force of a Point Load," ASME *Journal of Applied Mechanics,* Vol. 59, pp. xx–00.

Moran, B., and Shih, C. F., 1987, "Crack-Tip and Associated Domain Integrals From Momentum and Energy Balance," *Engineering Fracture Mechanics,* Vol. 27, pp. 615–642.

Nemeth, N. N., Mandersheid, J. M., and Gyekenyesi, J. P., 1989, "Ceramic Analysis and Reliability Evaluation of Structures (CARES)—User's Guide," NASA Technical Paper 2916.

Rourk, R. J., 1971, *Formulas for Stress and Strain,* 4th ed, McGraw-Hill, New York.

Selverian, J. H., ONeil, D. A., and Kang, S., 1992, *The American Ceramic Society Bulletin,* Vol. 71(9).

Selverian, J. H., O'Neil, D. A., and Kang, S., 1994, "Performance Testing and Strength Prediction of Ceramic-to-Metal Joints," ASME JOURNAL OF ENGINEERING FOR GAS TURBINES AND POWER, Vol. 116, pp. 622–628.

Yang, M., and Kim, K. S., 1993, "On the Behavior of Sub-interface Cracks With Crack-Face Contact," *Journal of Engineering Fracture Mechanics,* Vol. 44, No. 1, pp. 155–165.